Journal of Magnetism and Magnetic Materials 323 (2011) 1134–1139

Contents lists available at ScienceDirect

Journal of Magnetism and Magnetic Materials

journal homepage: www.elsevier.com/locate/jmmm

Micromagnetic study of magnetic domain structure and magnetization reversal in amorphous wires with circular anisotropy

I. Betancourt [a,*], G. Hrkac [b], T. Schrefl [b,c]

[a] Departamento de Materiales Metálicos y Cerámicos, Instituto de Investigaciones en Materiales, Universidad Nacional Autónoma de México, México D.F. 04510, Mexico
[b] Department of Engineering Materials, University of Sheffield, Mappin St., Sheffield S1 3JD, UK
[c] St. Pölten University of Applied Sciences, Austria

ARTICLE INFO

Article history:
Received 10 August 2010
Received in revised form
2 November 2010
Available online 10 December 2010

Keywords:
Magnetic domains
Amorphous wires
Micromagnetism
Circular anisotropy
Magnetization reversal of amorphous wires

ABSTRACT

In this work we present a detailed numerical investigation on the magnetic domain formation and magnetization reversal mechanism in sub-millimeter amorphous wires with negative magnetostriction by means of micromagnetic calculations. The formation of circular magnetic domains surrounding a multidomain axially oriented central nucleus was observed for the micromagnetic model representing the amorphous wire. The magnetization reversal explained by micromagnetic computations for the *M*–*H* curve is described in terms of a combined nucleation–propagation – rotational mechanism after the saturated state. Results are interpreted in terms of the effective magnetic anisotropy.

1. Introduction

Iron- and cobalt-based amorphous alloys in the form of thin metallic wires with typical diameters between 70 and 150 μm obtained by rapid solidification from the melt by means of the rotating-water-bath-melt-spinning process have been the subject of active research since the beginning of the 1990s due to their peculiar magnetic behavior, including (a) magnetic bistability, i.e. a very well defined rectangular *M*–*H* loop afforded by a single Barkhausen jump, and (b) the Mateucci effect, consisting of the generation of a voltage across the ends of a twisted wire when it is placed in an alternating magnetic field [1–4]. Both responses are intimately related with the distinctive, experimentally observed magnetic domain structure that characterizes this kind of materials: a central core with a longitudinal single domain structure surrounded by a sheath of perpendicular magnetization with either radial or circular orientation depending on the wire's saturation magnetostriction λ_s value, which contributes to the domain formation by means of the magnetoelastic coupling ($\lambda_s > 0$ for radial direction and $\lambda_s < 0$ for circular orientation, whereas vanishing λ_s destroys the single inner domain structure because of the facility to form new domain walls) [1–5]. These magnetic features have afforded the implementation of a variety of technological applications for these amorphous wires as active elements in magnetic sensors and/or transducer devices [1–4]. In this work we present a detailed numerical investigation on the magnetic domain formation and reversal mechanism in amorphous wires with $\lambda_s < 0$ by means of the continuum theory of micromagnetism.

2. Numerical method

Micromagnetic calculations are based on the dynamic magnetization description given by the Landau–Lifshitz Gilbert (LLG) equation of motion:

$$\frac{\partial \mathbf{M}}{\partial t} = -\gamma' \mathbf{M} \times \mathbf{H}_{\text{eff}} - \frac{\alpha \gamma'}{M_s} \mathbf{M}(\mathbf{M} \times \mathbf{H}_{\text{eff}}) \quad (1)$$

where α is the dimensionless damping constant, γ is the electron gyromagnetic ratio and $\gamma' = \gamma/(1+\alpha^2)$. The effective field $\mathbf{H}_{\text{eff}}$ comprises the following terms: the exchange field $\mathbf{H}_{\text{ex}} = (2A/M_s)\nabla^2 \mathbf{m}$ (where A is the exchange constant, M_s is the saturation magnetization and $\mathbf{m}$ is the unit vector along M_s), which keeps neighboring magnetic moments parallel to each other; the anisotropy field $\mathbf{H}_K = -(1/M_s)(\partial E_{anis}/\partial \mathbf{m})$ (with E_{anis} the anisotropy energy density), which aligns magnetic moments along specific directions; the magnetostatic field $\mathbf{H}_d = -(1/2)\nabla\phi$ (where ϕ is the scalar potential), which arises from the magnetization distribution itself and the externally applied field $\mathbf{H}_{\text{ext}}$ [6]. In order to use Eq. (1) for calculating the equilibrium magnetization in a cylindrical model representing an amorphous wire, the model was discretized into tetrahedral finite elements according to the Ritz–Galerkin weak formulation [6,7]. For each node of the finite element mesh, a magnetic moment vector and a magnetic scalar potential is defined. The magnetic scalar potential follows from the magnetostatic boundary value problem. Instead of extending the finite element mesh over a larger region outside the magnet, the boundary

* Corresponding author. Fax: +52 55 56161371.
E-mail address: israelb@correo.unam.mx (I. Betancourt).

0304-8853/$ - see front matter © 2010 Elsevier B.V. All rights reserved.
doi:10.1016/j.jmmm.2010.11.089

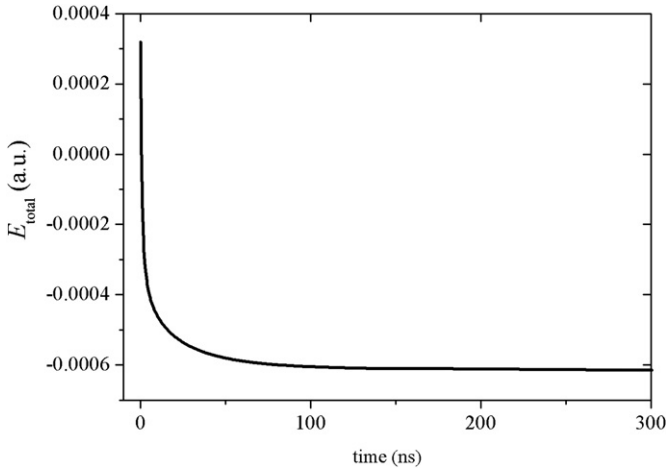

Fig. 1. Total magnetic energy E_{tot} as a function of time for the micromagnetic wire model.

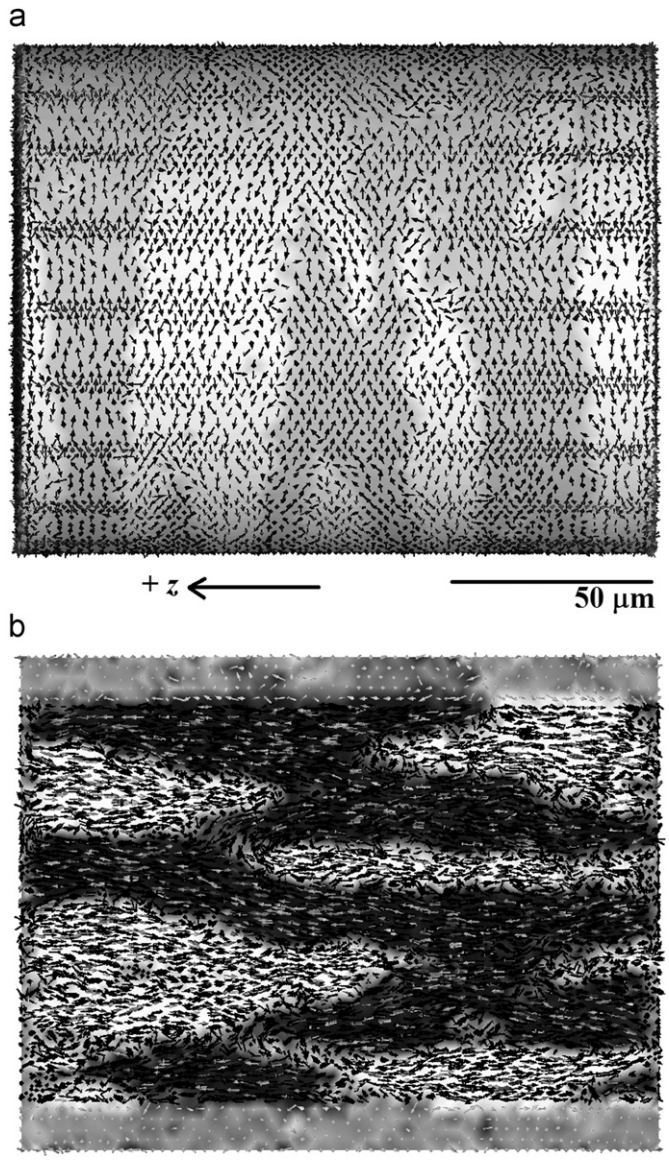

Fig. 2. (a) Surface equilibrium magnetization distribution for the amorphous wire model showing the formation of circular domains. (b) Transverse y–z profile. The color map indicates black areas pointing out to $+z$, while white zones point out to $-z$.

element method allows to treat the condition that the potential decays as $1/r$ with distance [8,9]. The space discretization of the LLG equation leads to a system of ordinary differential equations for the magnetic moment at the nodes of the finite element mesh. The equations are coupled by the exchange field and by the magnetostatic field and are solved by means of a time-integration technique, for which we used an implicit time-integration scheme with automatic time step control [10,11].

The amorphous wire model considered in this study consisted of a solid cylinder of radius $R_w = 60\ \mu m$ and length $150\ \mu m$ with its longitudinal axis oriented along the z direction. For this model we describe the magnetostriction by an effective magnetic anisotropy constant K_{eff}. This K_{eff} results from the magnetoelastic coupling between the internal stresses induced during the wire's fabrication process and the sign of λ_s, which in turn is determined by the chemical composition [1–4]. These internal stress variations in amorphous wires follow a rather complex distribution [12,13] with axial, radial and azimuthal components changing rapidly from positive (at the axial zone) to negative (at the surrounding shell), including maximum values at half the radius as well as on the wire's edges. Even zero stress value is expected at the very wire center [12,13]. For the micromagnetic wire model presented here, a single representative anisotropy strength K_{eff} is assumed. The intrinsic magnetic properties assigned to this model for mimicking real amorphous wires were taken as follows: $K_{eff} = 1000\ J/m^3$ following a circumferential orientation surrounding a central core of radius $R_c = 50\ \mu m$, for which its magnetization easy direction was set along the longitudinal cylinder axis. The K_{eff} value used in this work was determined experimentally for similar amorphous wires after suitable heat treatments [3,4,14] as well as the $R_c/R_w = 0.83$ ratio [14]. The saturation polarization $\mu_0 M_s$ was fixed as 0.8 T, the exchange constant A was taken as 1×10^{11} J/m and the damping constant α was of 0.01. The small α value used here is congruent with a homogenous amorphous structure, as it has been experimentally reported in FeB-based amorphous alloys [15].

A fundamental issue in this micromagnetic study is the exchange length L_{ex} for amorphous alloys, which determines to a large extent the viability of the numerical computations since this parameter determines the maximum size of the tetragonal finite elements used during the meshing process. According to the Random Anisotropy Model, L_{ex} for amorphous alloys can be established as follows [4,16–18] :

$$L_{ex} = \frac{16A^2}{9K_{loc}^2 d^3} \tag{2}$$

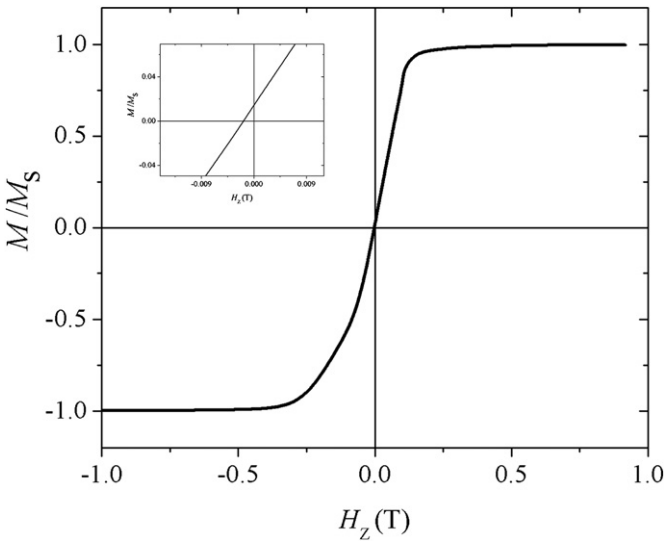

Fig. 3. Magnetization M–H curve for the amorphous wire model. The external field is applied along the $\pm z$ direction. The inset illustrates H_c and M_r/M_s values.

where A stands for the exchange constant and K_{loc} for the local anisotropy (i.e., the magnetic anisotropy of the short-range-order, local atom configuration characteristic of the amorphous structure) while d corresponds to the structural correlation length. For (Fe,Co)-based amorphous alloys typical A and K_{loc} values are $A \sim 10^{-11}$ J/m and $K_{loc} \sim 10^4$–10^5 J/m^3 [16–18], whereas d can be taken to be of the interatomic distance order, i.e., $d \sim 10^{-9}$ m [16,17]. Thus, by using these A, K_{loc} and d parameters in Eq. (2), we have $L_{ex} \approx 10$ μm. For this work we use $L_{ex} = 2.5$ μm. This exchange length affords the discretization of the microsized model cylinders described above with a mesh containing a number of finite elements around 600 000, well fitted for finite time computation purposes.

3. Results and discussion

Equilibrium magnetic states were calculated by integrating Eq. (1) for 300 ns, whereby the initial configuration was a random magnetization. At the equilibrium state for this time of integration, the total magnetic energy reaches a minimum, as shown in Fig. 1. The corresponding equilibrium magnetization distribution is shown in Fig. 2a, for which the formation of circularly oriented magnetic domains of alternate orientation on the cylinder surface is evident by the magnetic moment distribution represented by arrows. The circular domains have an average width of 22 μm and are formed across the entire external shell surrounding the inner zone of radius R_c. On the other hand, the central zone presents an axially oriented magnetization, as evidenced by the transverse y–z profile displayed in Fig. 2b, illustrating a multidomain structure comprising magnetic moments oriented along $\pm z$ directions (black arrows). A concurrent color map in this figure indicates black areas toward $+z$ and white areas toward $-z$. This equilibrium magnetic domain structure is congruent with experimental reports of amorphous wires with $\lambda_s < 0$ [1,2,5,19,20]. In addition, for real amorphous wires there is a critical length L_{cr}, which ensures the minimization of "closure domains" at both wire ends for the

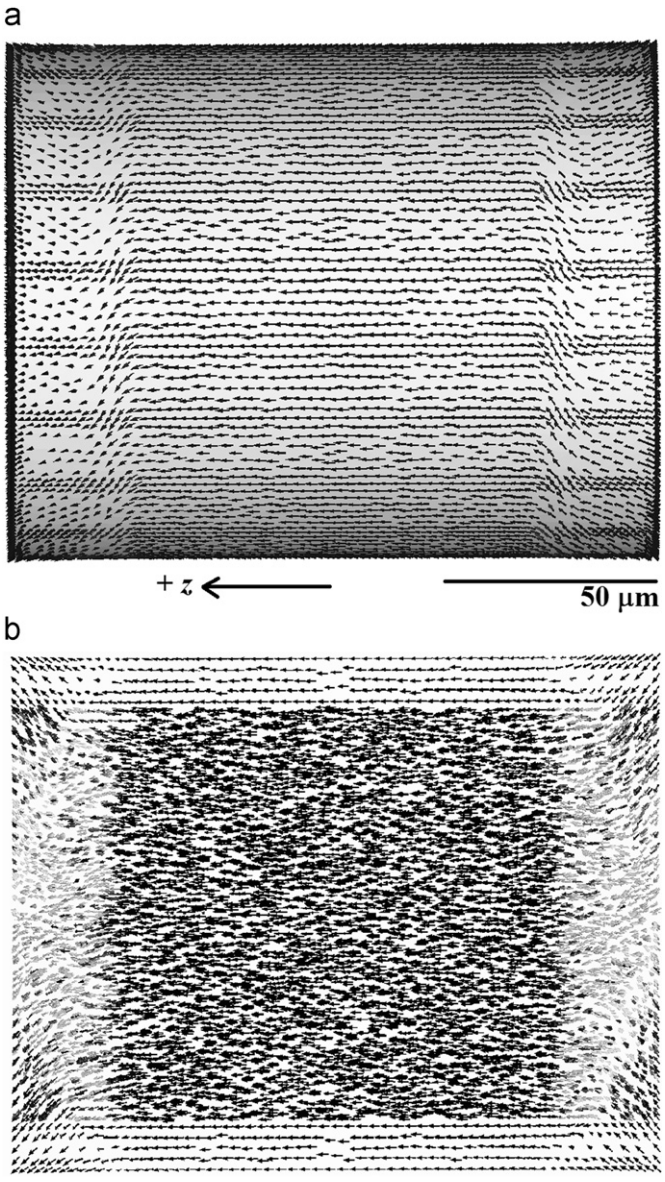

Fig. 4. Magnetization reversal process for the amorphous wire model at $H_z = 0.15$ T showing (a) nucleation of twisted zones near the edges of the wire model surface and (b) y–z profile illustrating the corresponding misalignment from $\pm z$ direction at the central core (black arrows indicate $+z$ direction, whereas any contrast in gray arrows indicates misaligned orientation).

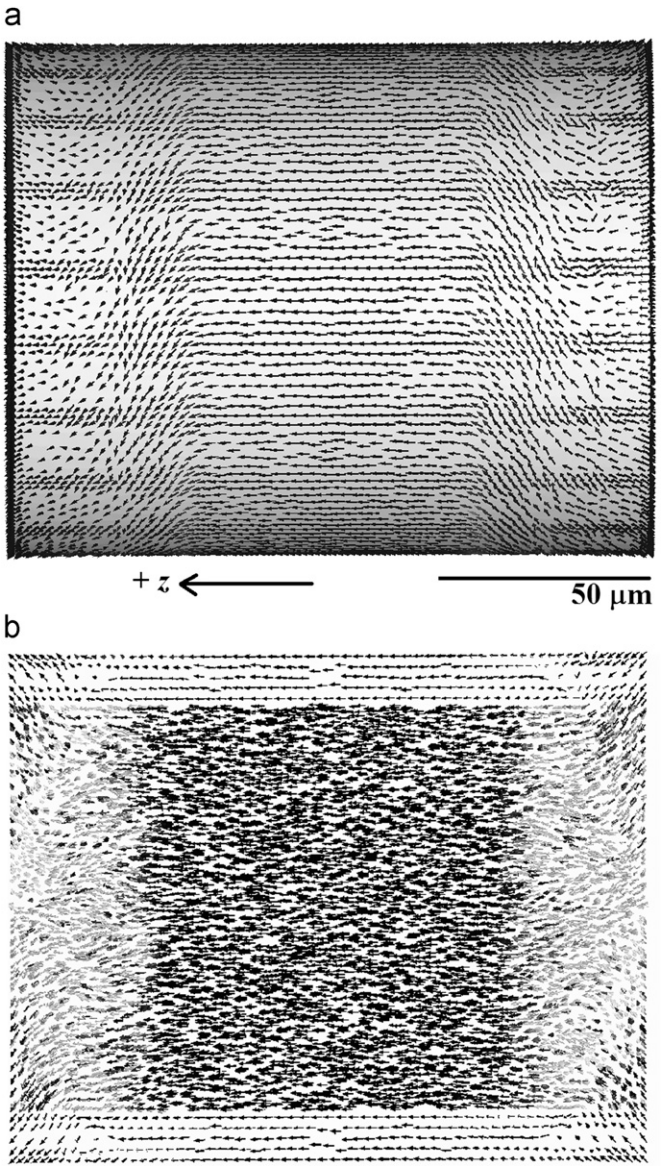

Fig. 5. Magnetization reversal process for the amorphous wire model at $H_z = 0.12$ T showing (a) the propagation of surface areas with twisted orientation toward the wire center and (b) y–z cut exhibiting the corresponding propagation from edges to center of misaligned zones from $+z$ direction at the central core (black arrows indicate $+z$ direction, whereas any contrast in gray indicates misaligned orientation).

condition $L > L_{cr}$ that leads to a saturated axial central zone [1,4]. Otherwise, for $L < L_{cr}$ the closure domains overlap to form multi-domain axial structures [1,4], as shown in this work for our wire model with $L \ll L_{cr}$. For developing a single domain axial zone, the L_{cr} should be over 70 mm for Fe-based and CoFe-based amorphous wires [1,4,21]. This L_{cr} is considerably larger than the dimensions of our cylindrical model and poses an overwhelming limit for time computation of micromagnetic simulations.

On the other hand, the magnetization M–H curve resulting from the application of an external field along $\pm z$ direction (with maximum $H_z = \pm 1.0$ T) is exhibited in Fig. 3, for which a quasi-non-hysteretic response is observed, characterized by a reduced coercive field H_c of 0.00017 T together with a minute relative remanence M_r/M_s value of 0.014 (Fig. 3 inset). This calculated M–H curve is consistent with experimental data corresponding to amorphous wires with well defined transverse circular anisotropy, for which the magnetization process was described in terms of near-reversible magnetization rotation from circular to axial direction under the effect of an increasing axial applied field [1].

For the present case, it is possible to describe the magnetization process in a more detailed way, since the micromagnetic calculation allows the monitoring of the reversal mechanism for small H_z steps. In this sense, a combined nucleation–propagation – rotational type mechanism was observed for the magnetization reversal after the saturated state along $+z$, as illustrated in Figs. 4–10. On the microwire surface the nucleation of twisted zones near the edges of the wire model begins at $H_z = 0.15$ T (Fig. 4a), while at the axial zone an equivalent misalignment from $\pm z$ direction is manifested according to the central y–z profile exhibited in Fig. 4b, for which black arrows correspond to $+z$ direction and any contrast in gray arrows indicates misaligned magnetic moments. The subsequent propagation of surface

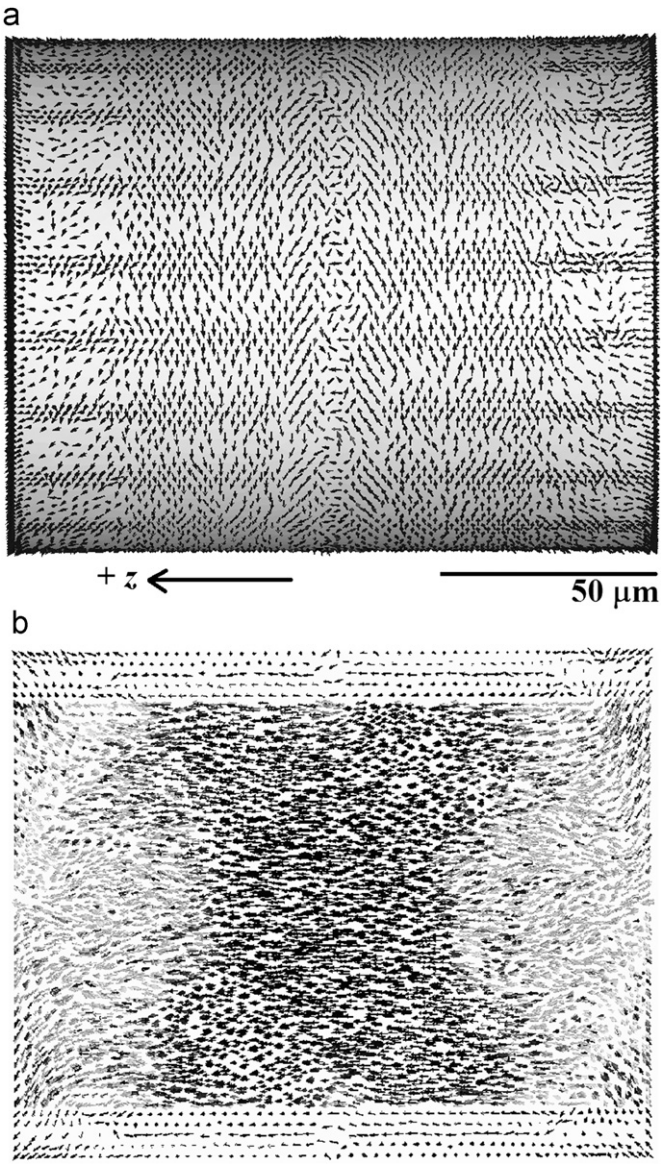

Fig. 6. Magnetization reversal process for the amorphous wire model at $H_z = 0.10$ T showing (a) formation of two circular domains of opposite orientation on wire surface separated by a domain wall structure on the middle, including twisted zones at the edges and (b) y–z profile exhibiting the evolution of misaligned areas from edges to center at the inner core (black arrows indicate $+z$ direction, whereas any contrast in gray indicates misaligned orientation).

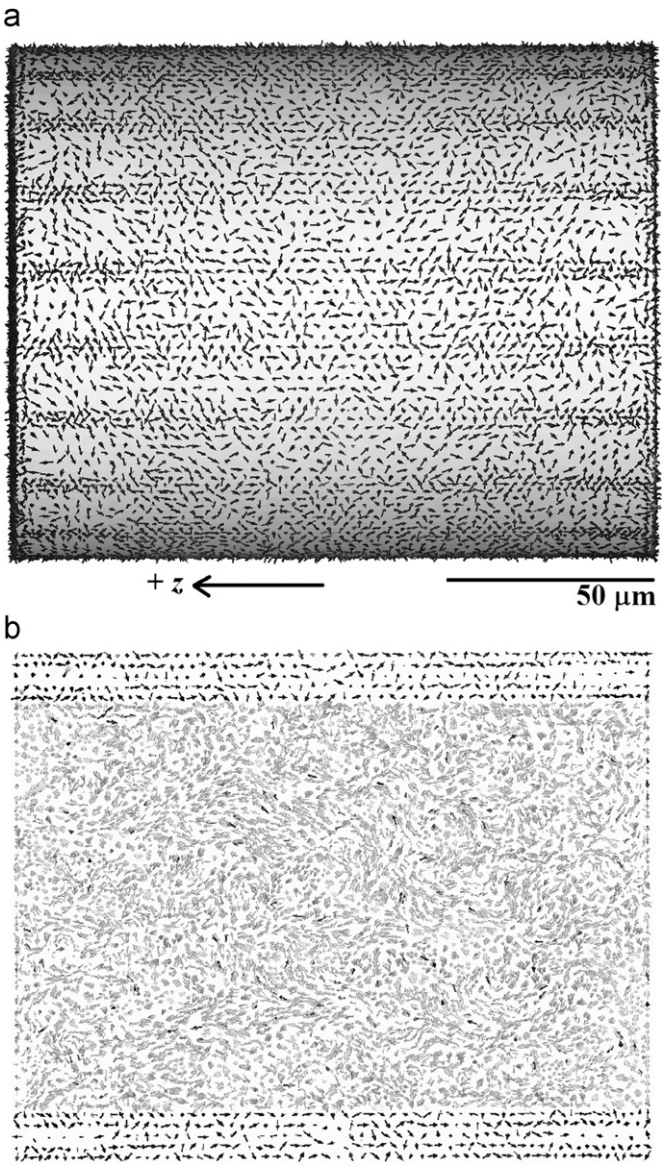

Fig. 7. Magnetization reversal process for the amorphous wire model at the remanent state $H_z = 0$ T showing (a) random magnetization distribution on the wire surface previous to rotational mechanism of magnetic moments toward $-z$ direction and (b) y–z profile of the central core exhibiting also a random distribution of magnetization (gray arrows indicate misaligned orientation from $\pm z$ direction).

areas with twisted orientation toward the wire center is illustrated in Fig. 5a for $H_z = 0.12$ T, whereas the central core shows an equivalent misalignment propagation from $+z$ direction according to the corresponding $y-z$ cut (Fig. 5b). Further reduction in H_z ($=0.10$ T) favors the formation of two circular domains of opposite orientation on wire surface separated by a domain wall structure on the middle of the model, including twisted zones at the edges, as shown in Fig. 6a, while at the central core the progressive misalignment from edges to center increases (Fig. 6b). For the remanent state ($H_z = 0$ T), a random magnetization distribution on the wire surface becomes evident in Fig. 7a, indicating the beginning of a progressive rotation mechanism of magnetic moments toward $-z$ direction. The associated $y-z$ profile of the central core (Fig. 7b) exhibits also a random magnetization previous to the rotational process in the direction of $-z$. Nevertheless, this magnetic configuration is not perfectly compensated as suggested by the non-zero relative remanence magnetization observed in the M–H curve of Fig. 3. After the remanent state, the magnetization reversal process is driven by the progressive rotation within the central core toward $-z$, as illustrated in Figs. 8–10, for which surface magnetization appears almost saturated (8a–10a), whereas the central core manifests a gradual reorientation from center to edges at $H_z = -0.30$ T (Fig. 8b), -0.35 T (Fig. 9b) and -0.60 T (Fig. 10b). This magnetization reversal observed for the amorphous wire model can be interpreted in terms of the effective magnetic anisotropy K_{eff}, which results from the magnetoelastic coupling between residual stresses induced during the wire's fabrication process and the sign of λ_s. The circular direction of K_{eff} on the model surface favors the nucleation of twisted zones after the saturated state and its further propagation to form two wide circular domains previous to the progressive rotation toward $-z$, while at the central core, the longitudinal anisotropy promotes a gradual rotation from $+z$ to $-z$ directions. These results are consistent with experimental reports for the nucleation of circular domains with opposite orientation, together with rotational process during the

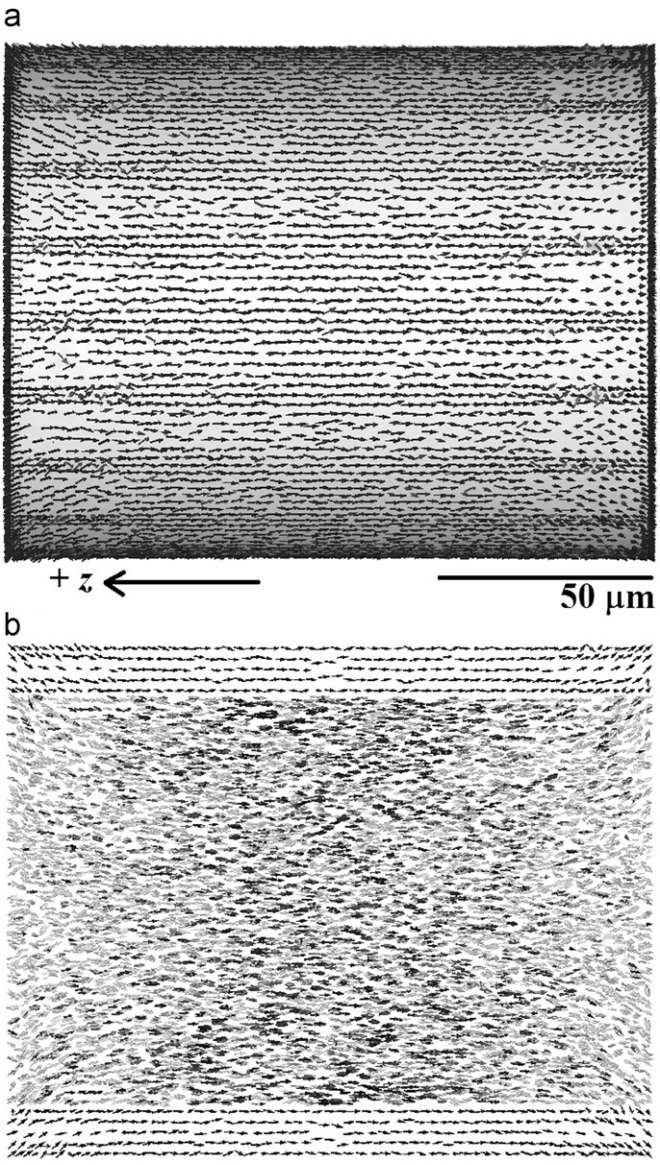

Fig. 8. Magnetization reversal process for the amorphous wire model at $H_z = -0.30$ T showing (a) surface magnetization with majority in $-z$ direction and (b) y–z cut of the central core exhibiting gradual reorientation from center to edges toward $-z$ direction (black arrows indicate $-z$ direction, whereas any contrast in gray indicates misaligned orientation).

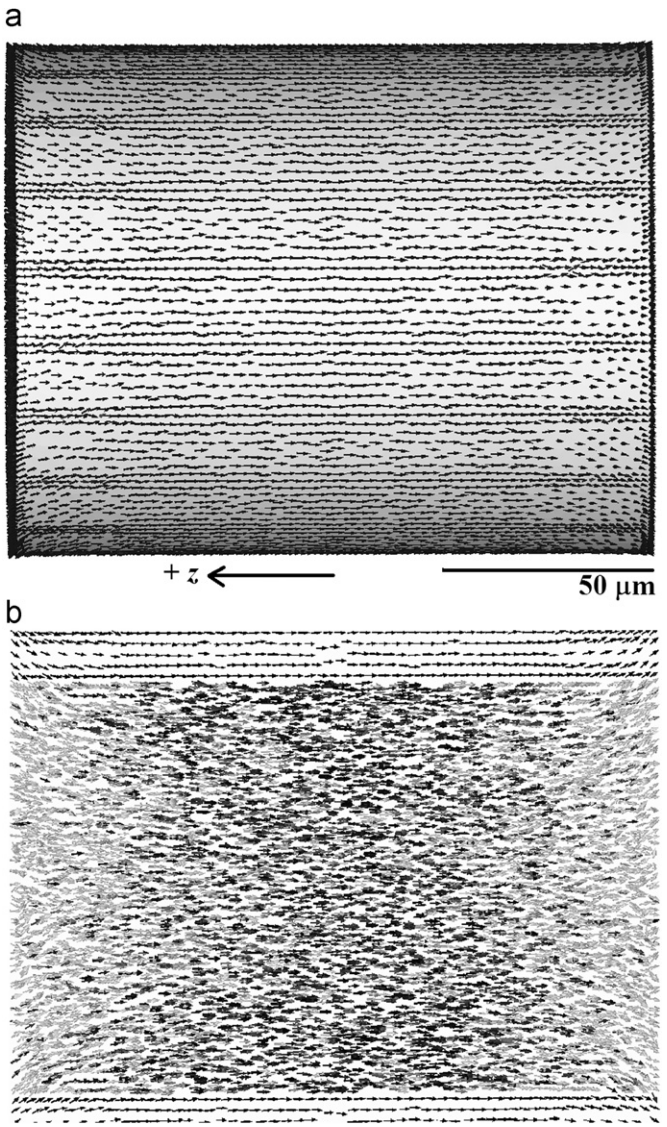

Fig. 9. Magnetization reversal process for the amorphous wire model at $H_z = -0.35$ T showing (a) surface magnetization with majority in $-z$ direction and (b) y–z profile of the central core exhibiting gradual reorientation from center to edges toward $-z$ direction (black arrows indicate $-z$ direction, whereas any contrast in gray indicates misaligned orientation).

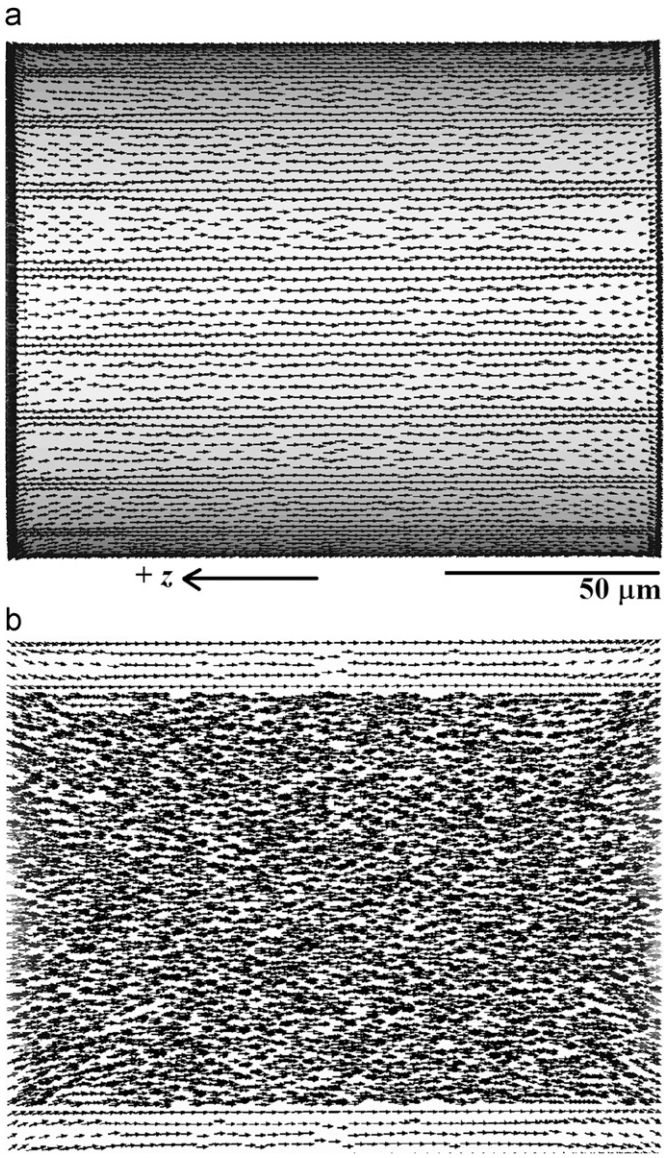

Fig. 10. Magnetization reversal process for the amorphous wire model at $H_z = -0.60$ T showing (a) surface magnetization with majority in $-z$ direction and (b) y–z cut of the central core exhibiting increased reorientation from center to edges toward $-z$ direction (black arrows indicate $-z$ direction, whereas any contrast in gray indicates misaligned orientation).

magnetization reversal observed in Co-based amorphous wires with negative magnetostriction by means of the magneto-optical Kerr effect [22].

4. Conclusions

The formation of circular magnetic domains around a longitudinally oriented multidomain central zone was observed for an amorphous wire model with $\lambda_s < 0$. The formation of magnetic domains is determined by the direction of the effective magnetic anisotropy K_{eff}, which also influences the magnetization reversal, for which nucleation, propagation and rotational features were observed.

Acknowledgments

I. Betancourt acknowledges the financial support from Research Grant IN106808 PAPIIT-UNAM, Mexico, as well as the supercomputing facilities of KanBalam, DGSCA-UNAM.

References

[1] M. Vazquez, Physica B 299 (2001) 302.
[2] M. Vazquez, Advanced magnetic microwires, in: H. Kronmüller, S. Parking (Eds.), Handbook of Magnetism and Advanced Magnetic Materials, vol. 5, Wiley, Chichester, 2007, p. 2193.
[3] H. Chiriac, T.A. Óvari, Amorphous wires and glass-covered wires, in: P. Tiberto, F. Vinai (Eds.), Magnetic Amorphous Alloys: Structural, Magnetic and Transport Properties, Research Signpost, Trivandrum, 2003, p. 111.
[4] A. Zhukov, J. Gonzalez, Amorphous and nanocrystalline soft magnetic materials: tailoring of magnetic properties, magnetoelastic and transport properties, in: Y. Liu, D.J. Sellmyer, D. Shindo (Eds.), Handbook of Advanced Magnetic Materials, vol. 3, Tsinghua University Press–Springer, New York, , 2006, p. 115.
[5] P.T. Squire, D. Atkinson, M.R.J. Gibbs, S. Atalay, J. Magn. Magn. Mater. 132 (1994) 10.
[6] J. Fidler, T. Schrefl, J. Phys. D: Appl. Phys. 33 (2000) R135.
[7] R.W. Chantrell, M. Wongsam, J. Fidler, T. Schrefl, Micromagnetics: finite element approach, in: K.H.J. Buschow (Ed.), Concise Encyclopedia of Magnetic and Superconducting Materials, 2nd ed., Elsevier, Amsterdam, , 2005, p. 298.
[8] D.R. Fredkin, T.R. Koehler, IEEE Trans. Magn. 26 (1990) 415.
[9] T.R. Koehler, Physica B 233 (1997) 302.
[10] G. Hrkac, T. Schrefl, O. Ertl, D. Suess, M. Kirschner, F. Dorfbauer, J. Fidler, IEEE Trans. Magn. 41 (2005) 3097.
[11] G. Hrkac, T. Schrefl, O. Ertl, D. Suess, M. Kirschner, F. Dorfbauer, J. Fidler, J. Appl. Phys. 97 (2005) 10E311.
[12] J. Liu, R. Malmhäll, L. Arnberg, S.J. Savage, J. Appl. Phys. 67 (1990) 4238.
[13] J. Velázquez, M. Vázquez, A. Hernando, H.T. Savage, M. Wun-Fogle, J. Appl. Phys. 70 (1991) 6525.
[14] F. Kinoshita, IEEE Trans. Magn. 26 (1990) 1786.
[15] P. Poulopoulos, S. Baskoutas, L.F. Kiss, L. Bujdosó, T. Kemény, F. Wilhelm, A. Rogalev, V. Kapaklis, C. Politis, M. Angelakeris, K. Saksl, J. Non-Cryst. Solids 354 (2008) 587.
[16] R. Alben, J.J. Becker, M.C. Chi, J. Appl. Phys. 49 (1978) 1653.
[17] G. Bertotti, E. Ferrara, F. Fiorillo, P. Tiberto, Mater. Sci. Eng. A 226–228 (1997) 603.
[18] R.C. OHandley, Modern Magnetic Materials, John Wiley & Sons, New York, 2000.
[19] M. Vázquez, A. Hernando, J. Phys. D: Appl. Phys. 29 (1996) 939.
[20] D. Atkinson, P.T. Squire, J. Magn. Magn. Mater. 140–144 (1995) 1901.
[21] A.M. Severino, C. Gomez-Polo, P. Marin, M. Vazquez, J. Magn. Magn. Mater. 103 (1992) 117.
[22] A. Chizhik, A. Zhukov, J.M. Blanco, J. Gonzalez, Physica B 299 (2001) 314.